Eur. J. Biochem. **271**, 2967–2975 (2004) © FEBS 2004 doi:10.1111/j.1432-1033.2004.04226.x

Structural characterization of photosystem II complex from red alga *Porphyridium cruentum* retaining extrinsic subunits of the oxygen-evolving complex

Ladislav Bumba[1,2], Helena Havelková-Doušová[3,4], Michal Hušák[4] and František Vácha[2,4]

[1]*Faculty of Biological Sciences, University of South Bohemia, České Budějovice;* [2]*Institute of Plant Molecular Biology, Academy of Sciences of the Czech Republic, České Budějovice;* [3]*Laboratory of Photosynthesis, Institute of Microbiology, Academy of Sciences of the Czech Republic, Třeboň;* [4]*Institute of Physical Biology, University of South Bohemia, České Budějovice, Czech Republic*

The structure of photosystem II (PSII) complex isolated from thylakoid membranes of the red alga *Porphyridium cruentum* was investigated using electron microscopy followed by single particle image analysis. The dimeric complexes observed contain all major PSII subunits (CP47, CP43, D1 and D2 proteins) as well as the extrinsic proteins (33 kDa, 12 kDa and the cytochrome c_{550}) of the oxygen-evolving complex (OEC) of PSII, encoded by the *psbO*, *psbU* and *psbV* genes, respectively. The single particle analysis of the top-view projections revealed the PSII complex to have maximal dimensions of 22×15 nm. The analysis of the side-view projections shows a maximal thickness of the PSII complex of about 9 nm including the densities on the lumenal surface that has been attributed to the proteins of the OEC complex. These results clearly demonstrate that the red algal PSII complex is structurally very similar to that of cyanobacteria and to the PSII core complex of higher plants. In addition, the arrangement of the OEC proteins on the lumenal surface of the PSII complex is consistent to that obtained by X-ray crystallography of cyanobacterial PSII.

Keywords: electron microscopy; membrane protein; photosynthesis; photosystem II; single particle image analysis.

Red algae are evolutionarily one of the most primitive eukaryotic algae. The photosynthetic apparatus of red algae appears to represent a transitional state between cyanobacteria and photosynthetic eukaryotes. The ultrastructure of red algal chloroplasts is similar to that of cyanobacteria. Thylakoid membranes of red algae are not differentiated into stacked and unstacked regions as found in higher plants and green algae [1,2]. Both cyanobacteria and the red algae contain phycobilisomes that serve as the primary light-harvesting antenna for photosystem II [3] instead of chlorophyll a/b (or chlorophyll a/c)-binding proteins reported in higher plants and algae [4–6]. However, the red algae, like all photosynthetic eukaryotes, contain intrinsic chlorophyll-based light-harvesting complex (LHC) associated with photosystem I (PSI) [6].

The process of oxygenic photosynthesis uses light energy to drive the synthesis of organic compounds and results in a release of molecular oxygen while the carbon dioxide is fixed from the atmosphere into the synthesized carbohydrates. Oxygenic photosynthesis is therefore essential for all life on Earth. It provides the energy in a form of reduced carbohydrates and the molecular oxygen necessary for all oxygen-respiratory based organisms. Central to this process is photosystem II (PSII), which catalyzes a series of photochemical reactions resulting a reduction of plastoquinone, oxidation of water, and formation of a transmembrane pH gradient.

PSII is a multicomponent protein complex that comprises more than 25 subunits (coded by *psbA–psbZ* genes); most of them are embedded in the thylakoid membrane [7–9]. All redox cofactors are bound to a central part of the complex formed by the reaction center D1 and D2 proteins associated with heterodimeric cytochrome b_{559} (cyt b_{559}) and PsbI protein [10]. The reaction center is surrounded by the chlorophyll a-binding inner antenna proteins CP47 and CP43 [11] together with several low-molecular mass proteins with unknown functions [12]. Water splitting is performed by a cluster of four Mn^{2+} ions coordinated with the D1 protein and located close to the inner, lumenal side of the thylakoid membrane [13]. Water oxidation requires presence of Ca^{2+} and Cl^- ions coordinated to extrinsic proteins that form, together with the Mn cluster, an oxygen-evolving complex (OEC) located on the lumenal side of the PSII complex (see Fig. 7) [14]. Among these extrinsic proteins only the 33 kDa protein, encoded by *psbO* gene, is common to all of the oxygen-evolving photosynthetic organisms [15]. In addition to the 33 kDa protein, higher plants and green algae contain the 23 kDa (PsbP) and 16 kDa (PsbQ) extrinsic proteins. In cyanobacteria and red algae, these proteins are missing and they are replaced by the cyt c_{550} and 12 kDa protein, encoded by *psbV* and *psbU*

Correspondence to L. Bumba, Institute of Plant Molecular Biology, Academy of Sciences, Branišovská 31, 370 05 České Budějovice, Czech Republic. Fax: + 420 38 5310356, Tel.: + 420 38 7775522, E-mail: bumba@umbr.cas.cz

Abbreviations: cyt, cytochrome; LHCI, light harvesting complex I; Mes, 2-morpholinoethanesulfonic acid; OEC, oxygen-evolving complex; PSI, photosystem I; PSII, photosystem II.

(Received 5 January 2004, revised 21 May 2004, accepted 25 May 2004)

genes, respectively [16,17]. In the red alga *Cyanidium caldarium*, the fourth additional extrinsic protein with a molecular mass of 20 kDa has been reported [18].

PSII also binds the peripheral antenna system, which absorbs the light energy and directs it to the photochemical reaction center. The antenna system of cyanobacteria and red algae is formed by water-soluble phycobilisomes. These supramolecular complexes are composed of phycobiliproteins with covalently attached open-chain tetrapyrroles [3]. The antenna system of higher plants and green algae consists of membrane-bound chlorophyll a/b-binding proteins coded by lhcb1–6 genes [4,5,8]. The Lhcb1 and Lhcb2 proteins form a major heterotrimeric light-harvesting complex of PS II (LHCII) whose structure was determined by electron [19] and X-ray [20] crystallography. The remaining minor Lhcb proteins are present in monomeric form and function as linker proteins between the trimeric LHC II and PS II core complex.

Low-resolution structural data of PSII have been obtained by means of electron microscopy and are reviewed in [8,21]. Principally, there are two types of PSII projections observed in electron microscope. They are called 'side views' and 'top views' and their frequency depends on the form of interaction between the PSII complex and the carbon on the support grid. 'Side views' are those PSII complexes attached to the microscopic grid by their side part that is originally embedded in the membrane, 'top views' are those attached to the grid by the outer membrane parts [22]. Single particle image analyses of various PSII preparations have revealed PSII to be present *in vivo* in the dimeric form. Three-dimensional (3D) structures of the PSII complexes have provided structural information about the OEC proteins of cyanobacteria [23], spinach [24] and the green alga *Chlamydomonas reinhardtii* [23]. Recently the 3D structural models of the dimeric PSII core complexes of spinach and cyanobacteria (*Synechococcus elongatus*, *Thermosynechococcus vulcanus*) have been derived by electron [25] and X-ray [26–28] crystallography, respectively. The models provide information on the arrangement of transmembrane helices as well as about the organization of the redox cofactors and chlorophyll a molecules. In the case of extrinsic subunits, there are divergences in the location of the subunits between cyanobacterial and higher plant-types OEC proteins [21].

In this paper we report structural maps of PSII complex isolated from the red alga *Porphyridium cruentum*. The structure has been obtained by electron microscopy and single particle image analyses of negatively stained preparations. The analyses of dimeric PSII complex reveal the location of the extrinsic OEC proteins on the lumenal surface of the PSII complex similar to that reported for the X-ray model of PSII from cyanobacteria.

Materials and methods

Growth conditions

The cells of *P. cruentum* Vischer 1935/107 (obtained from Culture Collection of Algal Laboratory, Trebon, Czech Republic; CCALA 415) were grown in glass tubes containing 250 mL artificial sea water medium [29] and bubbled with air enriched with 2% (v/v) CO_2. The alga was cultured under continuous illumination at an irradiation level of 30 μmol photons·m^{-2}·s^{-1} at 18 °C.

Isolation of thylakoid membranes

Thylakoid membranes were isolated by a modified method as described elsewhere [18]. All purification steps were carried out at low temperature (4 °C) under dim light conditions. The algal cultures were harvested in an exponential growth phase by centrifugation for 5 min at 6000 ***g***. Pelleted cells were twice washed in distilled water and then centrifuged for 5 min at 6000 ***g***. The resulting pellet was resuspended in buffer A containing 50 mM 2-morpholinoethanesulfonic acid (Mes) (pH 6.2), 20% (v/v) glycerol and sonicated in three cycles for 10 s. Cells were broken with glass beads 100–200 μm in diameter in a Beadbeater cell homogenizer (BioSpec Products, Inc., Bartlesville, OK, USA) for 10 cycles (15 s shaking with 2 min break). The suspension was sieved by buffer A through nylon cloth and unbroken cells were removed by centrifugation for 5 min at 6000 ***g***. The supernatant was then centrifuged for 60 min at 130 000 ***g*** (Beckmann SW 28 rotor) and the resulting pellet was resuspended at 50 mM Mes/NaOH (pH 6.2), 0.5 M sucrose, 2 mM Na_2EDTA. The homogenate was loaded on a cushion of 1.8 M sucrose in 50 mM Mes (pH 6.2) and centrifuged for 20 min at 150 000 ***g*** (Hitachi P70AT). The thylakoid membranes were harvested by a syringe from the green interphase and stored at −60 °C.

Isolation of PSII complex

Thylakoid membranes were solubilized with 1% *n*-dodecyl-β-D-maltoside in 50 mM Mes (pH 6.5) at a chlorophyll concentration of 1 mg·mL^{-1} chlorophyll a for 15 min. The unsolubilized material was removed by centrifugation for 30 min at 60 000 ***g*** and the supernatant was loaded onto a freshly prepared 0.1–1 M continuous sucrose density gradient prepared by freezing and thawing the centrifuge tubes filled with a buffer containing 20 mM Mes (pH 6.5), 0.5 M sucrose, 10 mM NaCl, 5 mM $CaCl_2$, 0.03% *n*-dodecyl-β-D-maltoside. The following centrifugation was carried out at 4 °C using a P56ST swinging rotor (Hitachi) at 150 000 ***g*** for 14 h. The lowest green band containing both photosystems was harvested with a syringe and loaded onto a DEAE Sepharose CL-6B (Pharmacia) anion-exchange column (10 × 100 mm) equilibrated by 50 mM Mes (pH 6.2), 5 mM $CaCl_2$, 10% glycerol, 0.03% *n*-dodecyl-β-D-maltoside. Complexes were eluted from the column with a linear gradient of 0–300 mM NaCl in 50 mM Mes (pH 6.2), 5 mM $CaCl_2$, 10% glycerol, 0.03% *n*-dodecyl-β-D-maltoside at a flow rate of 1 mL·min^{-1}. The nonbinding fraction eluted during sample loading was rich in PSI, whereas pure PSII was eluted at a concentration of 75 mM NaCl. The eluted complexes were concentrated by membrane filtration using Amicon 8010 concentrator (Millipore, Billerica, MA, USA).

Polyacrylamide gel electrophoresis

Protein composition was determined by SDS/PAGE using a 12–20% linear gradient of polyacrylamide gel [30] containing 6 M urea. Proteins in the gel were visualized either by Coomassie staining or silver staining kit (Amersham

Biosciences). A presence of cytochrome in a gel was detected by heme staining procedure. The gel was immersed into a solution containing 0.25% (w/v) 3,3′,5,5′-tetramethylbenzidine, 250 mM sodium acetate (pH 5.0) and 25% methanol for 60 min. The heme was visualized by an addition of 2% H_2O_2.

Pigment analysis

Chlorophyll concentrations were determined according to Ogawa and Vernon [31]. Room temperature absorption spectra were recorded with a UV300 spectrophotometer (Spectronic Unicam, Cambridge, UK). Fluorescent emission spectra were measured at liquid nitrogen temperature using a Fluorolog spectrofluorometer (Jobin Yvon, Edison, NJ, USA) with an excitation wavelength of 430 nm.

Oxygen evolution

Oxygen evolution was measured using a Clark-type oxygen electrode (Hansatech, Pentney, UK). Samples at a chlorophyll concentration of 10 μg chlorophyll·mL^{-1} were suspended in a medium containing 20 mM Mes (pH 6.5), 0.3 M sucrose, 20 mM $CaCl_2$, 10 mM $NaHCO_3$, 10 mM NaCl, supplemented with electron acceptors, 2,5-dichloro-*p*-benzoquinone at a concentration of 500 μM and ferricyanide at a concentration of 2.5 mM and illuminated with saturating white light.

Gel filtration chromatography

Gel filtration chromatography was performed using Superdex 200 H 10/30 column (Amersham Biosciences) connected to a HPLC pump (LCP 3001, Ecom, Czech Republic) and photodiode array detector Waters 996 (Waters, Milford, MA, USA). The column was equilibrated with 20 mM Mes (pH 6.5), 10 mM NaCl and 0.03% *n*-dodecyl-β-D-maltoside at flow rate of 0.5 mL·min^{-1}. Chromatograms were recorded at 435 nm. The column was calibrated with molecular mass standards (Sigma): thyroglobulin (669 kDa), apoferritin (443 kDa), β-amylase (200 kDa), alcohol dehydrogenase (150 kDa) in 20 mM Mes (pH 6.5), 10 mM NaCl and 0.03% *n*-dodecyl-β-D-maltoside.

Electron microscopy and image analysis

Freshly prepared complexes were obtained from gel filtration chromatography and immediately used for electron microscopy. The specimen was placed on glow-discharged carbon-coated copper grids and negatively stained with 2% uranyl acetate. Electron microscopy was performed with Philips TEM 420 electron microscope using 80 kV at 60 000× magnification. Micrographs were digitized with a pixel size corresponding to 0.51 nm at the specimen level. Image analyses were carried out using SPIDER software [32]. From 61 micrographs of the PSII preparation, about 7380 top-view and 3250 side-view projections were selected for analysis. The selected projections were rotationally and translationally aligned, and treated by multivariate statistical analysis in combination with classification [33,34]. Classes from each of the subsets were used for refinement of alignments and subsequent classifications. For the final sum, the best of the class members were summed using a cross-correlation coefficient of the alignment procedure as a quality parameter. The resolution of the images was calculated by using the Fourier ring correlation method [35].

Results

Three chlorophyll-containing fractions were resolved on sucrose density gradient after centrifugation of solubilized thylakoid membranes (fractions A–C, Fig. 1A). Fraction A in the upper part of the gradient contained 24% of total chlorophyll content and the rest of the chlorophyll was found in fraction B and fraction C in almost equal amounts. SDS/PAGE resolved many proteins in fraction A with prominent bands between 15 and 20 kDa corresponding to antenna polypeptides of LHCI [36,37]. Proteins of PSI and PSII complexes were missing in this green fraction but free PSII core antenna protein CP43 was detected (Fig. 1B, lane A).

The fractions B and C contained polypeptides of PSI and PSII complexes as indicated by SDS/PAGE and spectroscopic data. Both fractions contained a 60 kDa band typical for the PsaA/B reaction center proteins of PSI, and the CP47 and CP43 protein bands characteristic for the PSII core complex (Fig. 1B, lanes B and C). Fraction C, in addition, was enriched in proteins of the cyt b_6/f and ATP-synthase complex. The fluorescence spectrum of the fraction C had two maxima at 695 and 718 nm characteristic for PSII and PSI, respectively (Fig. 2B).

In order to isolate PSII, the fraction C from the gradient was loaded on anion-exchange column chromatography

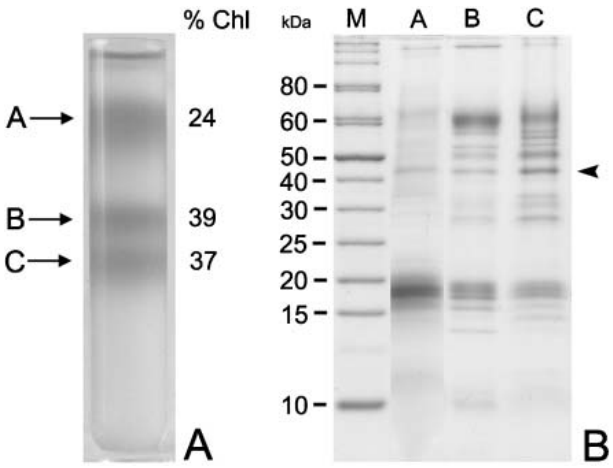

Fig. 1. Protein analysis of different pigment–protein complexes from thylakoid membranes of *P. cruentum* separated by sucrose density gradient. (A) Sucrose density gradient centrifugation of thylakoid membranes from *P. cruentum*. Thylakoid membranes were solubilized with *n*-dodecyl-β-D-maltoside and separated in a linear 0–1 M sucrose gradient. A pigment ratio of separated chlorophyll-containing bands is indicated on the right. (B) SDS/PAGE analysis of the three sucrose gradient bands A–C. Fractions were separated on a 12–20% denaturating gradient gel and Coomassie stained. Lane M, markers (molecular masses, in kDa, are indicated on the left); lanes A–C, fractions A–C from the sucrose density gradient. The arrowhead indicates the position of the CP43 subunit.

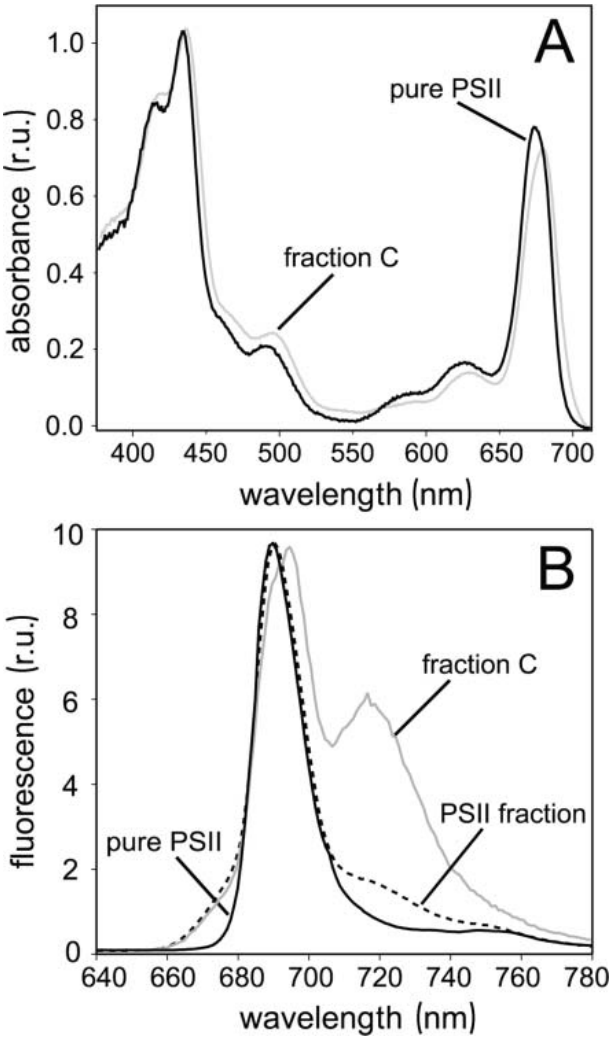

Fig. 2. Absorption and fluorescence spectra of different PSII preparations from *P. cruentum*. (A) Room temperature absorption spectra of purified PSII and sucrose density gradient fraction C. (B) 77K fluorescence emission spectra of the sucrose density gradient fraction C, the PSII fraction eluted from anion-exchange chromatography and pure PSII complex obtained by a gel filtration chromatography (Fig. 4). Spectra were normalized to the maxima of absorption and fluorescence, respectively.

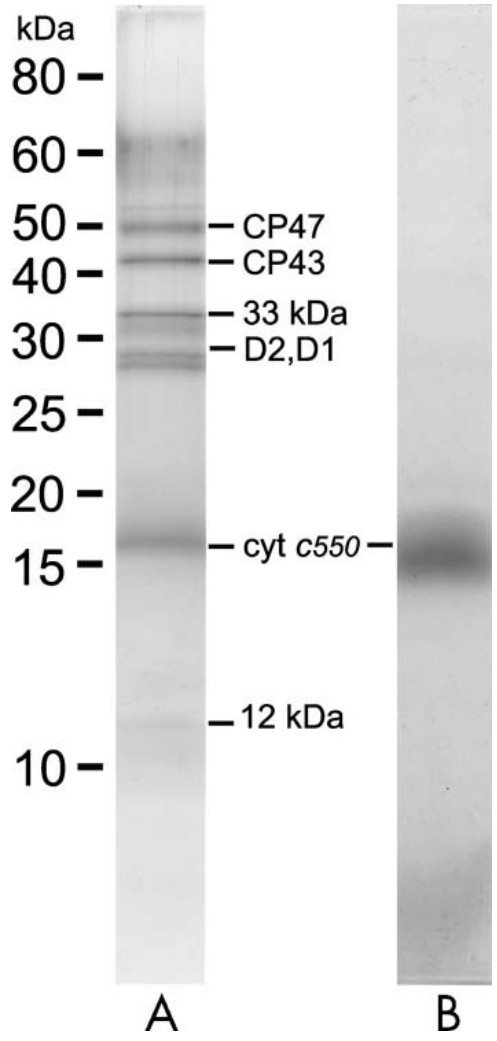

Fig. 3. SDS/PAGE analysis of partially purified PSII from *P. cruentum* using an anion-exchange column. The PSII fraction was separated on a 12–20% denaturating gradient gel. Proteins were detected by silver staining (A) and heme staining (B), respectively. Molecular mass markers are indicated on the left.

and the fractions were eluted with a linear gradient of 0–300 mM NaCl. SDS/PAGE and spectroscopic analyses showed that a majority of PSI was associated with the nonbinding fraction (not shown). The PSII fraction was eluted with a concentration of 75 mM NaCl. As shown in Fig. 3 (lane a), the PSII fraction contained the major subunits of PSII typical for red algal preparation [18]. It consists of the intrinsic subunits CP47, CP43, D2 and D1, and the extrinsic proteins of the oxygen-evolving complex the 33 kDa, cyt c_{550} and 12 kDa. The presence of the cyt c_{550} in the PSII fraction was confirmed by heme staining of the gel (Fig. 3B). However, after the anion-exchange chromatography step the PSII preparation was still slightly contaminated with PSI as indicated by a broad band on the SDS gel with a molecular mass of 60 kDa (Fig. 3A). Room temperature absorption spectrum of the PSII fraction is shown in Fig. 2A. The PSII fraction exhibited absorption maxima at 438 nm and 674 nm and lacked the significant absorbance around 550 nm indicating that the sample is free of phycobiliproteins. 77K fluorescence emission spectrum of PSII fraction from anion-exchange column showed a single emission peak with maximum at 692 nm characteristic for PSII [38]; the contamination by PSI is indicated by a small shoulder at 720 nm (Fig. 2B, dotted line).

The PSII fraction from anion-exchange column was further purified on gel filtration chromatography. Gel filtration analysis (Fig. 4) shows a major peak of PSII. A small shoulder at the front edge of the main peak of PSII represents the PSI contaminant. Samples of PSII complexes for electron microscopy were collected from the maximum of the main peak of the gel filtration. The 77K fluorescence emission spectrum of the main gel filtration peak of PSII (Fig. 2B, solid line) lacks the emission at 720 nm and indicates no contamination by PSI particles.

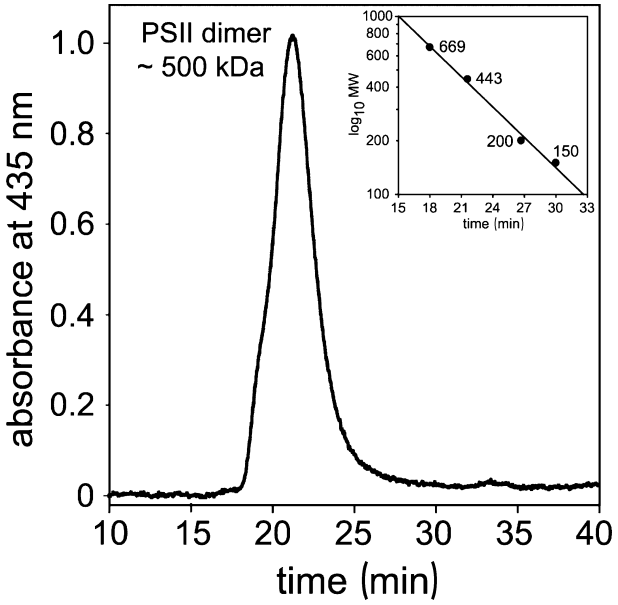

Fig. 4. Gel-filtration chromatography elution profile of partially purified PSII. The chromatogram was detected at 435 nm. The main peak running at 21 min corresponds to the PSII dimers with molecular mass of about 500 kDa. Inset, the calibration curve of standards with known masses: thyroglobulin (669 kDa), apoferritin (443 kDa), β-amylase (200 kDa), and alcohol dehydrogenase (150 kDa).

The isolated PSII particles were active in oxygen evolution and yielded 436 ± 52 μmol $(O_2)\cdot(\text{mg chlorophyll})^{-1}\cdot h^{-1}$. PSII complexes were negatively stained by uranyl acetate, visualized by electron microscopy and processed by image analysis. Typical electron microscopy images in Fig. 5 clearly show that the preparation contains dispersed particles with uniform size and shape and is almost free of contaminants.

To process the particle images by single particle analysis, a large data set was extracted from the images and the projections were aligned, treated with multivariate statistical analysis and classified into classes. After the classification steps, the top-view data set was decomposed into eight classes, six of which are presented in Fig. 4. The projections are very similar in the overall shape and size (Fig. 6A–C). All the classes had the same type of handedness, which indicates preferential binding of the particles by their stromal side to the carbon support film [39,40]. Small differences in the particle dimensions probably reflect a tilting of the particle on the electron microscopy grid. Although no symmetry has been imposed during the image analysis clearly twofold rotational symmetry around the center of the complex is visible indicating the dimeric nature of the PSII core complex. To obtain higher resolution of the averaged PSII particle dimer projections with a strong twofold rotational symmetry were pooled from the classes and the sum of the best images with imposed twofold symmetry are presented in Fig. 7A. The resolution of final projections calculated by means of the Fourier ring correlation method [35] and was found to be 26 Å. Overall, the averaged top-view projection of the PSII core complex indicate a trapezoid particle with a dimension of 22 × 15 nm (Fig. 6A). In about 12% of the data set a

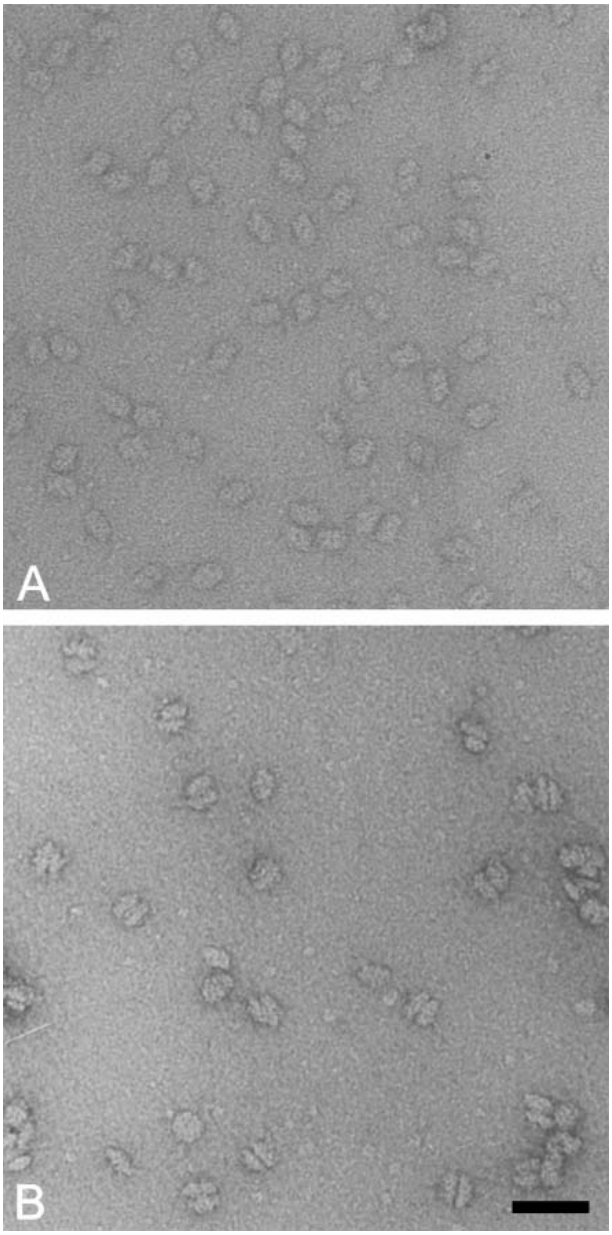

Fig. 5. Electron micrographs of isolated dimeric PSII complexes in their top-view (A) and in side-view (B) positions. Samples were negatively stained with 2% uranyl acetate. The scale bar represents 50 nm.

fragment with a significant reduction of a mass in upper part of the particle was observed (Fig. 6D).

The presence of millimolar concentration of divalent ions in the buffer induced the artificial aggregation of two single PSII complexes attached with their stromal surfaces. Because of a low affinity of the PSII lumenal surface to the support carbon film [39,40], the aggregates composed of two PSII dimers were observed in their side-view projections (Fig. 5B). For image analysis side-view projections were analyzed with masking out the contribution of the neighboring PSII particles. Thus, from a set of 3250 aggregates, 6500 'single' side-view projections were selected for image analysis. The classification of such images resulted in the set of six classes presented in Fig. 8. The main differences in the averaged

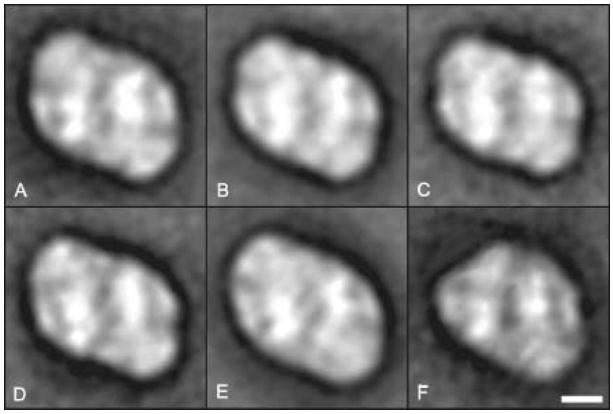

Fig. 6. Single particle analysis of top-view projections of *P. cruentum* PSII complexes. (A–F) The six classes obtained by classification of 7380 projections. Average projections represent dimeric PSII (A–E) and a fragment of dimeric PSII (F) lacking the CP43 subunit at upper left part of the complex. The projections are presented as facing from the lumenal side of the thylakoid membrane. The number of summed images is: 545 (A), 513 (B), 478 (C), 468 (D), 454 (E) and 276 (F). The scale bar represents 5 nm.

classes are related with distinct lengths of the particles. Whilst the overall length of the particles ranges between 15 nm (Fig. 8E,F) and 21 nm (Fig. 8A–D), an overall height of about 9 nm is constant in all the projections. As the lengths of the side-views correspond well with the length and width of particle in the top-view projection, the distinct lengths of the side views represent the particles that are attached with the longer or the shorter axis parallel to the support carbon film, respectively. Changes in length of the projections were also associated with variations in the appearance of the protrusions. The distances between the protrusions are proportional to the lengths of particles, which demonstrate an overlap of the extrinsic subunits in the different binding of the side views to the carbon support film.

Discussion

Here we report the isolation of the dimeric PSII core complex from the red alga *P. cruentum* retaining the proteins of oxygen-evolving complex (33 kDa, cyt c_{550}, 12 kDa). Such a complex from *P. cruentum* has already been isolated previously, however, without all of the extrinsic subunits [38]. The presence of cyanobacterial-type OEC proteins (i.e. the 33 kDa, cyt c_{550} and 12 kDa protein) and phycobilisomes as antennae in red algae instead of the 23 and 16 kDa proteins and LHCII complex found in green algae and higher plant PSII [14] suggests that the eukaryotic red algal PSII is closely related to prokaryotic cyanobacterial PSII rather than to PSII in higher plants. Gel filtration chromatography estimated the molecular mass of the

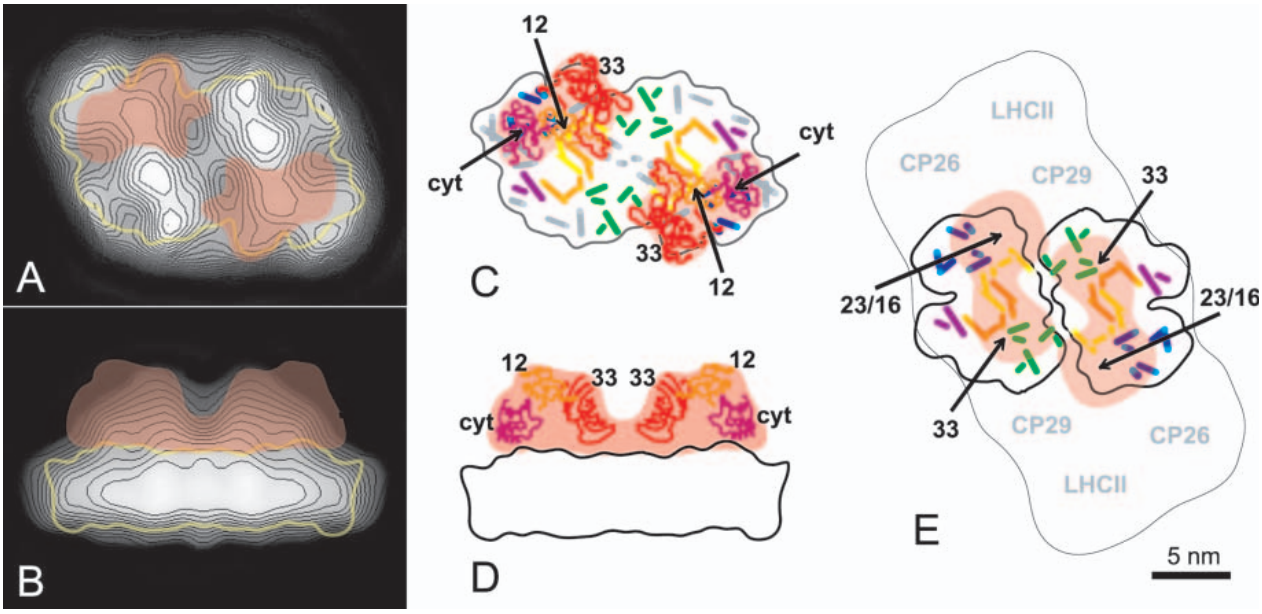

Fig. 7. Schematic representation of subunit organization of the extrinsic subunits on the lumenal side of dimeric PS II in the red alga *P. cruentum* (A,B), cyanobacteria (C,D) and in higher plants (E). The location of extrinsic subunits is indicated by red areas. Top-view (A) and side-view (B) projection map of negatively stained PSII core complex with imposed twofold rotational symmetry from *P. cruentum* superimposed with the cyanobacterial X-ray model of the PSII complex [from (C) and (D)]. Top-view (C) and side-view (D) projection maps of cyanobacterial dimeric PS II core complex obtained by X-ray crystallography. The coordinates are taken from Protein Data Bank (http://www.rcsb.org/pdb), code 1FE1 [26] and 1IZL [27]. The Cα backbone of the 33 kDa (dark red), cyt c_{550} (violet) and 12 kDa subunits (dark orange) are indicated. The underlying transmembrane α-helices are represented by columns and the assignment of individual proteins are depicted in different colors (D1, yellow; D2 orange; CP47, green; CP43, blue; cyt b_{559}, purple; unidentified helices, gray). (E) Top-view projection maps of the spinach PSII–LHCII supercomplex obtained by cryo-electron microscopy and 3D reconstitution [23]. The contour of the spinach dimeric PS II core complex [25] is overlaid to the supercomplex and the location of the antenna proteins is also indicated. The supercomplex is tilted in order to compare the differences in the organization of the OEC subunits on the lumenal surfaces between cyanobacteria (C,D) and higher plants (E). Scale bar is 5 nm.

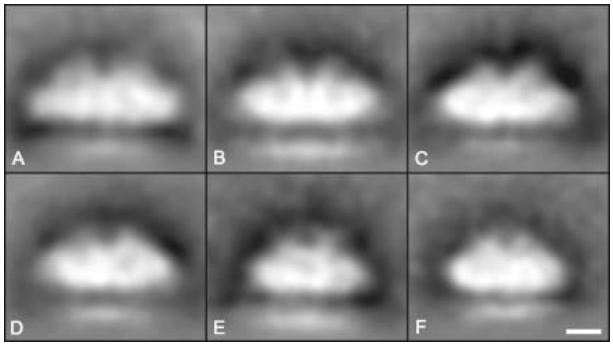

Fig. 8. Single particle analysis of side-view projections of *P. cruentum* PSII complexes. (A–F) The six classes found by classification of 6500 projections. The average images represent PSII complexes in their side-view projections. Proteins of the oxygen-evolving complex are visualized as a protrusion on the lumenal surface of the PSII complex. The distinct lengths of particles (E) and (F) are caused by tilting of the complexes. The number of summed images is: 437 (A), 408 (B), 378 (C), 362 (D), 427 (E) and 398 (F). The scale bar represents 5 nm.

oxygen evolving PSII complex from *P. cruentum* to be approximately 500 kDa (Fig. 4) that corresponds to the complex of PSII dimers from both cyanobacteria [39] and higher plants [41].

Electron microscopy with single particle analysis of the dimeric PSII complex isolated from *P. cruentum* revealed that the top- and side-view projections are very similar to those obtained from both cyanobacteria and higher plants [8,24,40]. The average top-view projection shows clear twofold rotational symmetry around the center of the complex indicating the dimeric nature of the PSII core complex. Each monomer unit contains five protein density areas separated by two areas of low-density (Fig. 6A–E) similar to the features in the top-view projections of the dimeric PSII core complex from *S. elongatus* [39].

In order to compare the PSII core complex from *P. cruentum* with that of cyanobacteria we have incorporated a model of transmembrane helix organization obtained by X-ray crystallography for *T. vulcanus* [27] into the projection map of the red alga taken from Fig. 6A. As it can be seen in Fig. 7A, the X-ray model well fits to the red algal projection map. As a consequence the incorporation of the X-ray model into the *P. cruentum* structure allows the identification of the missing fragment seen in Fig. 6F as the CP43 subunit. The CP43 subunit has been found to be a more loosely associated to PSII core complex [42]. The lack of the CP43 fragment in some part of the projections is also strengthened by the occurrence of the free CP43 subunit in the fraction A of the sucrose gradient (Fig. 1B, lane A). The absence of other peripheral densities in the top-view projection map of the red algal PSII core complex supports the evidence that no additional intrinsic antenna components are associated with the red algal PSII complex.

The side-view projections have been shown to provide an overview of the location of proteins of the OEC [24,39,43]. The OEC subunits are visualized as protrusions on the lumenal side of the PSII complex. The most abundant projection type of *P. cruentum* (Fig. 8A) is identical to the cyanobacterial side-view obtained previously by single particle analysis [39,40] and shows two separated protrusions symmetrically located with respect to the center of the complex. The inner part of the cyanobacterial protrusion has been previously identified as the 33 kDa extrinsic subunit, while the outer part is formed by cyt c_{550} and the 12 kDa subunit [39]. The presence of identical extrinsic subunits, as well as the similarities in the side-view projection maps in both red algae and cyanobacteria suggests uniformity in the arrangement of the OEC subunits. However, release-reconstitution experiments in both cyanobacterial and red algal PSII have shown that the binding patterns of the extrinsic proteins are different between these organisms. In cyanobacteria, cyt c_{550} can directly bind to PSII essentially independent on the presence of other extrinsic proteins [44], whereas effective binding of red algal cyt c_{550} to the red algal PSII requires the presence of all of the other extrinsic proteins [18].

The location of cyanobacterial OEC subunits has been also studied by 3D reconstruction of negatively stained PSII core complexes from *S. elongatus* [23]. The 3D reconstruction of cyanobacterial PSII has revealed the OEC subunits as protrusions on the lumenal surface of the complex, which were in relative positions to those determined for the OEC proteins of spinach [24] and *Chlamydomonas reinhardtii* [23] (Fig. 7E). Based on these similarities it has been concluded that the 33 kDa protein is located over the CP47/D2 side of the cyanobacterial PSII core complex, whereas the cyt c_{550}/12 kDa are positioned over the D1 protein. These results are in contrast to the structural data derived from the X-ray diffraction analysis of the PS II crystals [26–28]. As shown in Fig. 7C,D, location of the extrinsic subunits derived from X-ray structure is indicated as red areas over the model of transmembrane helix organization. The model shows that the 33 kDa protein is located over the D1 protein of the PSII core complex, whereas cyt c_{550} kDa is situated over the CP43/cyt b_{559} side [27]. The 12 kDa protein is located between the 33 kDa protein and cyt c_{550} but apart from the lumenal surface (Fig. 7D). Considering the X-ray structural data [27] within the 3D-reconstitution model obtained by single particle analysis [23] the discrepancies in location of the OEC proteins should be outlined. The protrusion that has been assigned to 33 kDa protein in the 3D reconstitution model is present in the X-ray structure, however, it has been found to correspond to the large lumenal loop of the CP47 instead of the 33 kDa protein. These results suggest that the structural patterns of the OEC proteins differs and do not form basic structural feature of the PS II core complex among the cyanobacteria, green algae and higher plants [21].

In order to further locate the OEC proteins in red algae we have overlaid the side-view projection of the cyanobacterial X-ray model [27] into the *P. cruentum* side-view projection. As shown in Fig. 7B, the contours of red algal projection are of similar size and shape to those of cyanobacterial, in particular to the structural features of the protrusions, allowing the identification of the extrinsic subunits. In conjunction with the X-ray model derived from cyanobacteria [27], we conclude that in red algae, the inner part of the lumenal protrusion can be assigned to accommodate the 33 kDa extrinsic protein whereas the outer part consists of the cyt c_{550} subunit. The 12 kDa subunit is not completely superimposed by the red algal projection, however, it is present in the complex as indicated by SDS/

PAGE (Fig. 3A). Considering the red algal side-view data with those of the X-ray model we were able to suggest location of the red algal OEC proteins in their top-view projection. Along with the location of the extrinsic subunit in the cyanobacterial X-ray model [27], we suppose that the red algal 33 kDa protein is located over the D1 protein of the PSII core complex, whereas cyt c_{550} kDa is situated over the CP43/cyt b_{559} side (Fig. 7A). This organization is supported by the analysis of the side-view projections with their shorter lengths. As can be seen in Fig. 8, an apparent depression between the two lumenal protrusions can be recognized mostly in each side-view projections, independently on their lengths. A comparison of these side-view projections with those of the cyanobacterial model with corresponding particle lengths clearly suggests an identical location of the extrinsic subunits between cyanobacteria and red algae (not shown). Such arrangement is also consistent with cross-reconstitution experiments, which indicate that the red algal OEC proteins were able to bind to cyanobacterial PSII complex, leading to a partial restoration of oxygen evolution [45].

In conclusion, we suggest that the overall organization of the transmembrane helices in the red algal PSII complex is very similar to that of cyanobacteria and to the PSII core complex from higher plants. The presence of the cyanobacterial-type extrinsic proteins of oxygen evolving complex (the 33 kDa, cyt c_{550} and 12 kDa) in the red algae instead of the 23 and 16 kDa proteins found in higher plant suggests uniformity in the arrangement of the OEC subunits between cyanobacteria and red algae, and probably within all phycobilisomes-containing organisms. Evolutionary replacement of the cyanobacterial-type extrinsic OEC subunits for the higher plant-type in higher plants and green algae may reflect changes in antennae composition of PSII, the substitution of phycobilisome antennae for the intrinsic chlorophyll-binding proteins.

Acknowledgements

The authors wish to thank Drs Josef Komenda and Michal Koblizek for their critical reading of the manuscript. We also gratefully acknowledge the financial support of the Ministry of Education, Youth and Sports of the Czech Republic, LN00A141 and CEZ 12300001.

References

1. Gantt, E. (1994) Supramolecular membrane organization. In *The Molecular Biology of Cyanobacteria* (Bryant, D.A., ed.), pp. 139–216. Kluwer Academic Publishers, Dordrecht, the Netherlands.
2. Mustardy, L. & Garab, G. (2003) Granum revisited: a three-dimensional model – where things fall into place. *Trends Plant. Sci.* **8**, 117–122.
3. Mörschel, E. (1991) The light-harvesting antennae of cyanobacteria and red algae. *Photosynthetica* **25**, 137–144.
4. Green, B.R. & Durnford, D.G. (1996) The chlorophyll-carotenoid proteins of oxygenic photosynthesis. *Annu. Rev. Plant Physiol. Plant Mol. Biol.* **47**, 685–714.
5. Bassi, R., Sandona, D. & Croce, R. (1997) Novel aspects of chlorophyll a/b-binding proteins. *Physiol. Plant.* **100**, 769–779.
6. Durnford, D.G., Deane, J.A., Tan, S., McFadden, G.I., Gantt, E. & Green, B.R. (1999) A phylogenetic assessment of the eukaryotic light-harvesting antenna proteins, with implications for plastid evolution. *J. Mol. Evol.* **48**, 59–68.
7. Hansson, O. & Wydrzynski, T. (1990) Current perceptions of Photosystem II. *Photosynth. Res.* **23**, 131–162.
8. Hankamer, B., Boekema, E.J. & Barber, J. (1997) Structure and membrane organization of Photosystem II in green plants. *Ann. Rev. Plant. Physiol. Plant. Mol. Biol.* **48**, 641–671.
9. Barber, J., Nield, J., Morris, E.P., Zheleva, D. & Hankamer, B. (1997) The structure, function and dynamics of Photosystem II. *Physiol. Plant.* **100**, 817–827.
10. Nanba, O. & Satoh, K. (1987) Isolation of a Photosystem II reaction center consisting of D1 and D2 polypeptides and cytochrome b_{559}. *Proc. Natl Acad. Sci. USA* **84**, 109–112.
11. Bricker, T.M. & Frankel, L.K. (2002) The structure and function of CP47 and CP43 in Photosystem II. *Photosynth. Res.* **72**, 131–146.
12. Hankamer, B., Morris, E.P., Nield, J., Carne, A. & Barber, J. (2001) Subunit positioning and transmembrane helix organisation in the core dimer of Photosystem II. *FEBS Lett.* **504**, 142–151.
13. Renger, G. (2001) Photosynthetic water oxidation to molecular oxygen: apparatus and mechanism. *Biochim. Biophys. Acta* **1503**, 210–228.
14. Seidler, A. (1996) The extrinsic polypeptides of Photosystem II. *Biochim. Biophys. Acta* **1277**, 35–60.
15. Bricker, T.M. & Frankel, L.K. (1998) The structure and function of the 33 kDa extrinsic protein of Photosystem II: a critical assessment. *Photosynth. Res.* **56**, 157–173.
16. Shen, J.R., Ikeuchi, M. & Inoue, Y. (1992) Stoichiometric association of extrinsic cytochrome c_{550} and 12-kDa protein with a highly purified oxygen-evolving Photosystem II core complexes from *Synechococcus vulcanus*. *FEBS Lett.* **301**, 145–149.
17. Enami, I., Murayama, H., Ohta, H., Kamo, M., Nakazato, K. & Shen, J.R. (1995) Isolation and characterization of a Photosystem II complex from the red alga *Cyanidium caldarium*: association of cytochrome c_{550} and a 12 kDa protein with the complex. *Biochim. Biophys. Acta* **1232**, 208–216.
18. Enami, I., Kikuchi, S., Fukuda, T., Ohta, H. & Shen, J.R. (1998) Binding and functional properties of four extrinsic proteins of Photosystem II from a red alga, *Cyanidium caldarium*, as studied by release-reconstitution experiments. *Biochemistry* **37**, 2787–2793.
19. Kühlbrandt, W., Wang, D.N. & Fujiyoshi, Y. (1994) Atomic model of plant light-harvesting complex by electron crystallography. *Nature* **367**, 614–621.
20. Liu, Z.F., Yan, H.C., Wang, K.B., Kuang, T.Y., Zhang, J.P., Gui, L.L., An, X.M. & Chang, W.R. (2004) Crystal structure of spinach major light-harvesting complex at 2.72 angstrom resolution. *Nature* **428**, 287–292.
21. Bumba, L. & Vácha, F. (2003) Electron microscopy in structural studies of Photosystem II. *Photosynth. Res.* **77**, 1–19.
22. Bumba, L., Hušák, M. & Vácha, F. (2004) Interaction of Photosystem 2-LHC2 supercomplexes in adjacent layers of stacked chloroplast thylakoid membranes. *Photosynthetica* **42**, in press.
23. Nield, J., Kruse, O., Ruprecht, J., da Fonseca, P., Büchel, C. & Barber, J. (2000) Three-dimensional structure of *Chlamydomonas reinhardtii and Synechococcus elongatus* Photosystem II complexes allows for comparison of their oxygen-evolving complex organization. *J. Biol. Chem.* **275**, 27940–27946.
24. Nield, J., Orlova, E.V., Morris, E.P., Gowen, B., van Heel, M. & Barber, J. (2000) 3D map of the plant Photosystem II supercomplex obtained by cryoelectron microscopy and single particle analysis. *Nat. Struct. Biol.* **7**, 44–47.
25. Hankamer, B., Morris, E.P., Nield, J., Gerle, C. & Barber, J. (2001) Three-dimensional structure of the Photosystem II core dimer of higher plants determined by electron microscopy. *J. Struct. Biol.* **135**, 262–269.

26. Zouni, A., Witt, H.T., Kern, J., Fromme, P., Krauss, N., Saenger, W. & Orth, P. (2001) Crystal structure of Photosystem II from *Synechococcus elongatus* at 3.8 Å resolution. *Nature* **409**, 739–743.
27. Kamiya, N. & Shen, J.R. (2003) Crystal structure of oxygen-evolving Photosystem II from *Thermosynechococcus vulcanus* at 3.7 Å resolution. *Proc. Natl Acad. Sci. USA* **100**, 98–103.
28. Ferreira, K.N., Iverson, T.M., Maghlaoui, K., Barber, J. & Iwata, S. (2004) Architecture of the photosynthetic oxygen-evolving center. *Science* **303**, 1831–1838.
29. Jones, R.H., Speer, H.L. & Curry, W. (1963) Studies on the growth of the red alga *Porphyridium cruentum*. *Physiol. Plantarum* **20**, 697–705.
30. Laemmli, U.K. (1970) Cleavage of structural proteins during the assembly of the head of bacteriophage T4. *Nature* **227**, 680–685.
31. Ogawa, T. & Vernon, L.P. (1971) Increased content of cytochromes 554 and 562 in *Anabaena variabilis* cells grown in the presence of diphenylamine. *Biochim. Biophys. Acta* **226**, 88–97.
32. Frank, J., Radermacher, M., Penczek, P., Zhu, J., Li, Y.H., Ladjadj, M. & Leith, A. (1996) SPIDER and WEB: processing and visualization of images in 3D electron microscopy and related fields. *J. Struct. Biol.* **116**, 190–199.
33. Van Heel, M. & Frank, J. (1981) Use of multivariate statistics in analyzing the images of biological macromolecules. *Ultramicroscopy* **6**, 187–194.
34. Harauz, G., Boekema, E. & van Heel, M. (1988) Statistical image analysis of electron micrographs of ribosomal subunits. *Methods Enzymol.* **164**, 35–49.
35. Van Heel, M. (1987) Similarity between images. *Ultramicroscopy* **21**, 95–100.
36. Wolfe, G.R., Cunningham, F.X., Durnford, D., Green, B.R. & Gantt, E. (1994) Evidence for a common origin of chloroplasts with light-harvesting complexes of different pigmentation. *Nature* **367**, 566–568.
37. Tan, S., Wolfe, G.R., Cunningham,F.X. Jr & Gantt, E. (1995) Decrease of polypeptides in the PSI antenna complex with increasing growth irradiance in the red alga *Porphyridium cruentum*. *Photosynth. Res.* **45**, 1–10.
38. Wolfe, G.R., Cunningham, F.X., Jr, Grabowski, B. & Gantt, E. (1994) Isolation and characterization of Photosystem I and II from red alga *Porphyridium cruentum*. *Biochim. Biophys. Acta* **1188**, 357–366.
39. Kuhl, H., Rögner, M., van Breemen, J.F.L. & Boekema, E.J. (1999) Localization of cyanobacterial Photosystem II donor-side subunits by electron microscopy and the supramolecular organization of Photosystem II in the thylakoid membrane. *Eur. J. Biochem.* **266**, 453–459.
40. Boekema, E.J., Hankamer, B., Bald, D., Kruip, J., Nield, J., Boonstra, A.F., Barber, J. & Rögner, M. (1995) Supramolecular structure of the Photosystem II complex from green plants and cyanobacteria. *Proc. Natl Acad. Sci. USA* **92**, 175–179.
41. Hankamer, B., Nield, J., Zheleva, D., Boekema, E.J., Jansson, S. & Barber, J. (1997) Isolation and biochemical characterization of monomeric and dimeric Photosystem II complexes from spinach and their relevance to the organization of Photosystem II *in vivo*. *Eur. J. Biochem.* **243**, 422–429.
42. Komenda, J. & Masojidek, J. (1995) Functional and structural changes of the Photosystem II complex induced by high irradiance in cyanobacterial cells. *Eur. J. Biochem.* **233**, 677–682.
43. Boekema, E.J., Nield, J., Hankamer, B. & Barber, J. (1998) Localization of the 23-kDa subunit of the oxygen evolving complex of Photosystem II by electron-microscopy. *Eur. J. Biochem.* **252**, 268–276.
44. Shen, J.R. & Inoue, Y. (1993) Binding and functional properties of two new extrinsic components, cytochrome c_{550} and 12-kDa protein, in cyanobacterial Photosystem II. *Biochemistry* **32**, 1825–1832.
45. Enami, I., Yoshihara, S., Tohri, A., Okumura, A., Ohta, H. & Shen, J.R. (2000) Cross-reconstitution of various extrinsic proteins and Photosystem II complexes from cyanobacteria, red algae and higher plants. *Plant Cell Physiol.* **41**, 1354–1364.